RSC Advances

PAPER

View Article Online
View Journal | View Issue

Cite this: *RSC Adv.*, 2025, **15**, 41995

Phyto-engineered Pd-doped WO_3 nanocomposite *via Anisomeles indica* leaf extract: a recyclable heterogeneous catalyst for aqueous Petasis reaction, photocatalytic dye degradation, and antibacterial applications

Nilesh Pandit,[a] Avdhut Kadam,[a] Avinash Survase,[b] Prit Ashara,[c] Avdhut Patil,[d] Chaitali Bagade,[e] Sarika Patil[fg] and Santosh Kamble *[fg]

Received 12th September 2025
Accepted 18th October 2025

DOI: 10.1039/d5ra06905j

rsc.li/rsc-advances

The development of multifunctional nanocomposites through green chemistry approaches has gained significant attention for promoting sustainable synthetic methodologies and environmental remediation. In this work, a green and sustainable route was employed for the synthesis of a Pd-doped-WO_3 nanocomposite using *Anisomeles indica* leaf extract as a natural reducing and stabilizing agent. The nanocomposite was synthesized under mild, aqueous-phase conditions without the use of toxic chemicals. Characterization by FTIR (Fourier Transform Infrared Spectroscopy), XRD (X-ray Diffraction), SEM (Scanning Electron Microscopy), and EDX (Energy Dispersive X-ray Spectroscopy) confirmed the successful formation of well-dispersed Pd nanoparticles within the WO_3 matrix. The XRD analysis revealed that the WO_3 crystallized in a monoclinic phase (JCPDS no. 00-043-1035). The optimized composition with ~5 wt% Pd demonstrated superior multifunctional performance. Specifically, the (3 mol%) Pd–WO_3 nanocomposite served as an efficient recyclable catalyst for the Petasis reaction in aqueous medium, a highly active photocatalyst for dye degradation under sunlight, and a potent antibacterial agent against both Gram-positive and Gram-negative bacteria. The present work highlights its dual potential for environmental and biomedical applications. This green-synthesized Pd-doped WO_3 nanocomposite provides a sustainable solution for organic transformations, environmental remediation, and microbial control.

1 Introduction

The development of sustainable and efficient synthetic methodologies has significantly advanced through multicomponent reactions (MCRs), which enable the direct assembly of complex molecules from simple precursors in a single step.[1,2] Among these, the Petasis reaction has gained increasing attention due to its high functional group tolerance, mild reaction conditions,[3] and compatibility with aqueous media, making it a valuable tool for the synthesis of biologically active amines and amino acid derivatives.[4] Recent studies have demonstrated its utility in pharmaceutical and agrochemical synthesis, particularly when catalyzed by transition metals such as palladium and gold.[5,6] However, the widespread application of this reaction is often hindered by the limited recyclability and high cost of homogeneous catalysts, prompting a shift toward heterogeneous alternatives that offer enhanced sustainability and ease of separation.[7]

Anisomeles indica is a perennial herb that is commonly used in traditional medicines throughout South Asia, and recently it has been explored for its rich phytochemicals like flavonoids, phenolic acids, and glycosides, which have strong antioxidant and reducing properties.[8] The entire plant has been found to contain several bioactive constituents, primarily terpenoids such as anisomelic acid, ovatodiolide, 4,7-oxycycloanisomelic acid, and iso-ovatodiolide. Additionally, it possesses phytosterols like β-sitosterol and stigmasterol, along with flavonoids including flavones and apigenin. The plant also produces a volatile essential oil as part of its secondary metabolites.[9] A

[a]*Department of Chemistry, Yashavantrao Chavan Institute of Science, Constituent College, Karmaveer Bhaurao Patil University, Satara-415001, Maharashtra, India*
[b]*Department of Microbiology, Yashavantrao Chavan Institute of Science, Constituent College, Karmaveer Bhaurao Patil University, Satara-415001, Maharashtra, India*
[c]*Department of Biotechnology, Vyavasayi Vidya Pratishthan Engineering College, Gujarat 360005, India*
[d]*Department of Botany, Yashavantrao Chavan Institute of Science, Constituent College, Karmaveer Bhaurao Patil University, Satara-415001, Maharashtra, India*
[e]*Department of Chemistry, Shivaji University Kolhapur, Maharashtra, India*
[f]*Karmaveer Bhaurao Patil University, Satara-415001, Maharashtra, India. E-mail: santosh.san143@gmail.com*
[g]*Department of Chemistry, Sadguru Gadge Maharaj College, Karad-415124, Maharashtra, India*

total of fourteen phytochemical constituents were successfully isolated and characterized from the methanolic extract of the whole plant of *Anisomeles indica*. Like pedalitin, apigenin, ovatodiolide, methylgallate, apigenin 7-O-glucuronide, calceolarioside, cistanoside F, betonyoside A, campneoside II, acteoside, isoacteoside, and terniflorin.[10] Some early studies have shown its usefulness in making metal and metal oxide nanoparticles with good control over their size and shape.[11] But, its use in making hybrid nanocomposites for catalytic purposes is still not much explored. The different secondary metabolites present in *Anisomeles indica* leaf extract give a natural stabilizing and capping medium, which helps in forming well-dispersed and stable Pd-doped-WO_3 nanocomposites. This make new chances for combining traditional herbal sources with advanced catalyst designs.

The design of multifunctional nanocomposites has gained increasing attention due to their potential in catalysis, photocatalysis, and biomedical applications. Among various metal oxides, tungsten trioxide (WO_3) is considered a promising candidate because of its relatively narrow band gap (2.4–2.8 eV), excellent redox stability, and ability to utilize visible light, offering advantages over classical oxides such as TiO_2 and ZnO that are largely UV-active.[12,13] Despite these merits, pure WO_3 exhibits inherent drawbacks, including rapid electron–hole recombination, moderate surface area, and weak adsorption capacity for organic pollutants, which significantly restrict its efficiency in catalytic and photocatalytic processes.[14] To overcome these limitations, modification strategies such as metal doping, nanocomposite formation, and coupling with noble metals have been extensively explored.

In this context, noble metal incorporation has emerged as one of the most effective approaches to improve the photocatalytic and catalytic efficiency of WO_3. Noble metals act as electron sinks, enhance charge separation, and introduce active catalytic sites. Among them, palladium (Pd) is particularly attractive because of its high activity in C–C and C–N bond-forming reactions, strong ability to mediate electron transfer, and relatively lower cost compared to other noble metals such as Pt or Au.[15,16] Moreover, Pd-modified WO_3 has demonstrated enhanced activity in photocatalysis and organic transformations, owing to synergistic effects between Pd nanoparticles and the WO_3 matrix.[17,18]

Several synthetic methods, including hydrothermal,[19] sol–gel,[20] ultrasonication,[21] solvothermal[22] and chemical reduction approaches,[23,24] have been reported for the fabrication of Pd–WO_3 nanocomposites. While these routes often yield materials with improved performance, they suffer from drawbacks such as the use of toxic chemicals, harsh reaction conditions, energy-intensive steps, and limited recyclability. These challenges underline the importance of developing alternative, environmentally benign approaches that align with green chemistry principles.

In this work, we have reported a green and sustainable method for the synthesis of Pd-doped-WO_3 nanocomposite using *Anisomeles indica* leaf extract, and explored its multifunctional catalytic applications. The synthesized nanocomposite demonstrated excellent performance as a heterogeneous catalyst for Petasis reactions in aqueous hydrotropic medium, efficient photocatalytic degradation of synthetic dyes, and significant antibacterial activity against both Gram-positive and Gram-negative strains. The catalyst showed high stability, strong reusability, and minimal metal leaching even after multiple cycles, highlighting its practical utility in organic synthesis, environmental remediation, and antimicrobial applications. Notably, this is the first report of *Anisomeles indica*-mediated synthesis of Pd-doped-WO_3 nanocatalyst, offering a scalable and eco-friendly approach that bridges green chemistry, nanotechnology, and biomedical relevance.

2 Materials and methods

2.1 Materials

All chemicals used in this study, including methylene blue dye, palladium acetate, and sodium tungstate dihydrate, are of analytical grade and are purchased from Sigma-Aldrich and used without further purification.

2.2 Instrumentation

A range of analytical techniques was employed to thoroughly investigate the structural, morphological, compositional, and functional properties of the synthesized nanocomposite and its products. The crystalline structure of the Pd-doped-WO_3 nanomaterial was confirmed using X-ray diffraction (XRD) analysis performed on a BRUKER AXS D8 Advance diffractometer with Cu Kα radiation (λ = 1.54 Å) operating at 40 kV. Functional group identification was carried out using Fourier Transform Infrared Spectroscopy (FT-IR) on a Lambda Scientific FT-IR 7600 instrument. The surface morphology of the nanocomposite was examined through Scanning Electron Microscopy (SEM) using a JEOL JSM-IT200 microscope. Elemental composition and distribution were determined by Energy Dispersive X-ray Spectroscopy (EDX) integrated with the SEM system. To confirm the structure of the organic transformation products, both ^{1}H and ^{13}C Nuclear Magnetic Resonance (NMR) spectroscopy were employed using a Bruker AC spectrometer operating at 400 MHz for ^{1}H and 100 MHz for ^{13}C, with $CDCl_3$ as the solvent and tetramethylsilane (TMS) as the internal reference. All spectral data and graphical representations were analysed and plotted using OriginPro 2024 (64 bit) SR1 software.

2.3 Photocatalytic activity of Pd-doped-WO_3 in the degradation of methylene blue dye

To study the photocatalytic performance of Pd-doped-WO_3 NCs for the degradation of methylene blue dye, 1 mg of Pd-doped-WO_3 NCs was added to 100 mL of freshly prepared dye solution (10 ppm). This solution was marked as the test solution. Then this test solution was exposed to the sunlight. Further, for the comparative study, the dye solution without a catalyst (control) was also exposed to sunlight radiation. From the entire mixture of the test sample, a 5 mL solution was withdrawn at 5 minute intervals and centrifuged at 15 000 rpm for 25 minutes. The absorbance of the test sample supernatant was recorded *via*

a UV-Vis spectrophotometer. The degradation percentage of the dye was measured using eqn (1)

$$\text{Methylene blue degradation } (\%) = \frac{(C_0 - C_t)}{C_0} \times 100 \quad (1)$$

where, C_0 – pure dye solution, initial absorbance without catalyst, and C_t – dye absorbance with catalyst at time t, the first order kinetic reaction rate constant 'k_{app}' was calculated *via* eqn (2).[25]

$$\ln\left(\frac{C_t}{C_0}\right) = -k_{app}t \quad (2)$$

2.4 Analysis of biodegraded dye

The supernatant collected after degradation at 0–60 min was subjected to different analysis techniques. The absorption spectrum change study using a UV-Vis spectrophotometer. The metabolites formed after degradation of the MB dye were extracted using ethyl acetate. The rotatory evaporator is used to evaporate organic solvents. Dilute the dried degraded materials in a small quantity of methanol and use as a sample for TLC and HPLC analysis. Isocratic H_2O-2690 system with double absorbance sensor consists of a C18 column (4.6 × 250 mm) with HPLC grade methanol and H_2O as a mobile phase used in HPLC analysis. TLC was carried out using a stationary phase silica gel coated on an aluminum plate with a mobile phase of methanol and distilled water (D.W.) in a 9 : 1 concentration.

2.5 Antibacterial activity of Pd-doped-WO_3 NPs

The microbial cultures inoculums were prepared in sterile distilled water. The nutrient agar plates were used as a medium for bacterial growth. The *S. aureus*, *B. cereus*, *P. vulgaris*, and *S. typhimurium* cultures were spread on sterile nutrient agar plates. Wells are prepared in these plates using a sterile cork-borer having a size of 6 mm. 100 μg mL^{-1} synthesized material was dispersed in the sterile distilled water with the help of a micropipette. The plates were incubated at 37 °C for 24 h, to test antibacterial activity.[26]

3 Experimental

3.1 A collection of plants

The leaf samples of *Anisomeles indica* were collected from the forests of Ingaloon, Tal-Junnar, in the Pune district, Maharashtra 410509, India (lat 19.197472, long 73.707503) on 19 October 2024.

3.2 Preparation of plant extract

Mature and healthy leaves of *Anisomeles indica* were thoroughly washed with tap water, then air-dried under shaded laboratory conditions, and finally ground into a fine powder using a mechanical grinder. The powdered plant material (5 g) was subjected to extraction using a Soxhlet apparatus with 100 mL of distilled water as the solvent. The extraction was carried out for five complete cycles to ensure optimal recovery of water-soluble constituents.

3.3 Preparation of Pd(0) nanoparticles

A 0.05 M solution of palladium acetate was first prepared in distilled water. To this, 25 mL of *Anisomeles indica* leaf extract was added dropwise under continuous ultrasonication for 40 min. The mixture was then subjected to further ultrasonication at 60 °C for an additional hour. The reduction of Pd^{2+} to Pd(0) was indicated by a gradual color change from pale yellow to dark brown. The resulting colloidal suspension was centrifuged, and the solid product was collected and dried at room temperature to obtain the phyto-reduced Pd(0) nanoparticles.

3.4 Preparation of WO_3 nanoparticles

A 0.05 M aqueous solution of sodium tungstate dihydrate was prepared in distilled water, resulting in a pale-yellow solution. To this solution, 25 mL of *Anisomeles indica* leaf extract was added, and the mixture was subjected to ultrasonication at 80 °C for 1 hour. The resulting colloidal suspension was then centrifuged, and the precipitate was washed three times with distilled water to remove residual impurities. The obtained solid was dried at room temperature and subsequently calcinated at 600 °C for 2 hours to yield WO_3 nanoparticles.

Interestingly, under these mild synthesis conditions, the phytochemicals present in *Anisomeles indica* extract did not reduce W^{6+} ions from sodium tungstate to metallic tungsten. Instead, WO_3 nanoparticles were formed through hydrolysis and condensation of tungstate species, while phytochemicals most likely acted as stabilizing and capping agents for the oxide matrix.[27,28] This behavior contrasts with the same extract's ability to reduce Pd^{2+} to Pd^0 nanoparticles, highlighting its selective reducing nature depending on the metal ion system.

3.5 Preparation of Pd-doped-WO_3 nanocomposite

Pd-doped-WO_3 nanocomposite was synthesized by doping pre-synthesized Pd(0) nanoparticles into WO_3 under ultrasonication. Initially, both Pd(0) and WO_3 nanoparticles were prepared separately using *Anisomeles indica* leaf extract through a green synthesis approach. For the fabrication of the composite, 20 mg of Pd(0) nanoparticles and 400 mg of WO_3 nanoparticles (maintaining a 1 : 20 w/w ratio) were dispersed in 50 mL of deionized water. The dispersion was subjected to ultrasonication for 1 hour to ensure uniform distribution and strong interaction between Pd and WO_3 particles. After completion, the mixture was centrifuged, and the collected Pd-doped-WO_3 nanocomposite was washed several times, then dried at 60–70 °C. The final dry material was stored in a clean, airtight glass vial for use in catalytic, photocatalytic, and antibacterial applications. This environmentally friendly method offers a scalable and efficient route to produce Pd-doped-WO_3 nanocatalysts.

3.6 Procedure for synthesis of alkylaminophenols

A mixture containing 3 mL of 20% aqueous sodium *p*-toluenesulfonate (NaPTS), amine (1 mmol), and aldehyde (1 mmol) was stirred for 15–20 minutes at room temperature. Subsequently,

3 mol% of the Pd-doped-WO_3 nanocomposite catalyst was added, followed by the addition of boronic acid (1 mmol). The reaction mixture was then stirred at 60 °C, and the progress was monitored using thin-layer chromatography (TLC) with *n*-hexane and ethyl acetate (8 : 2) as the mobile phase. Upon completion, the catalyst was separated *via* simple filtration. The obtained alkylaminophenol products were dried and purified, followed by characterization using spectroscopic techniques such as FTIR, ^{1}H NMR, and ^{13}C NMR.

4 Result and discussion

4.1 Characterization of nanocatalysts

4.1.1 FT-IR analysis. The FTIR spectra (Fig. 1) of WO_3 and Pd-doped-WO_3 nanoparticles exhibit characteristic absorption bands that provide insights into their structural and surface features. A broad band observed at 3446 cm^{-1} in the WO_3 spectrum corresponds to O–H stretching vibrations, indicating the presence of surface hydroxyl groups or adsorbed water molecules. This band becomes less intense in Pd–WO_3, suggesting reduced surface hydroxylation due to Pd doping. The noticeable appearance or increased intensity of bands at 2932 cm^{-1} (C–H stretching) and 1339 cm^{-1} (C–N or C–O stretching) in the Pd-doped-WO_3 spectrum compared to pure WO_3 suggests chemical interaction of palladium species with bio-organic molecules from the plant extract and possible modification of the WO_3 matrix. These spectral changes, along with shifts in peak positions, support the successful incorporation of palladium into the WO_3 lattice, though further confirmed by XRD. A band at 1517 cm^{-1}, prominent in WO_3, corresponds to aromatic C=C stretching vibrations, likely from plant-derived compounds. In Pd–WO_3, the peak intensities in this region vary, indicating interaction of Pd with these organic molecules. The band at 1339 cm^{-1} is related to C–O stretching, while the band at 1047 cm^{-1} corresponds to W–O–W vibrations, confirming the structural integrity of the tungsten oxide matrix. Overall, Pd doping results in slight shifts and intensity changes in the spectra, indicating successful incorporation of Pd into the WO_3 lattice and its interaction with bio-organic components from the plant extract.

4.1.2 XRD. X-ray diffraction (XRD) analysis was conducted to examine the phase structure and crystallinity of the synthesized Pd-doped-WO_3 nanomaterial (Fig. 2). The black XRD pattern corresponds to the Pd-doped-WO_3, showing several well-defined peaks that align with two standard reference patterns: monoclinic WO_3 (JCPDS no. 00-043-1035) and metallic palladium (JCPDS no. 01-085-0624). The diffraction peaks marked with pink squares are characteristic of monoclinic WO_3, confirming the formation of a well-crystallized tungsten oxide phase. Additional peaks marked with blue circles match the standard pattern for elemental Pd, the presence of peaks at 2θ values 29.38°, 55.02°, indicating the successful incorporation of palladium in the composite, within the WO_3 lattice. The absence of any extra peaks suggests that no impurity phases are present, and the material is phase pure. The overall sharp and intense reflections also indicate high crystallinity, which is

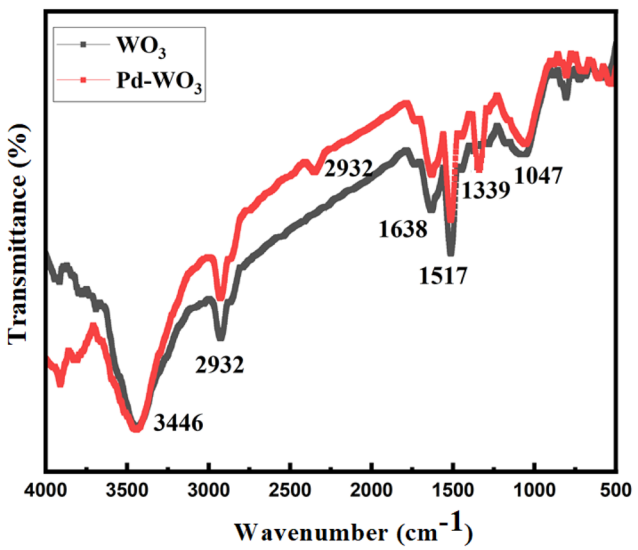

Fig. 1 FTIR spectrum of Pd-doped-WO_3 nanocomposite synthesized using *Anisomeles indica* extract.

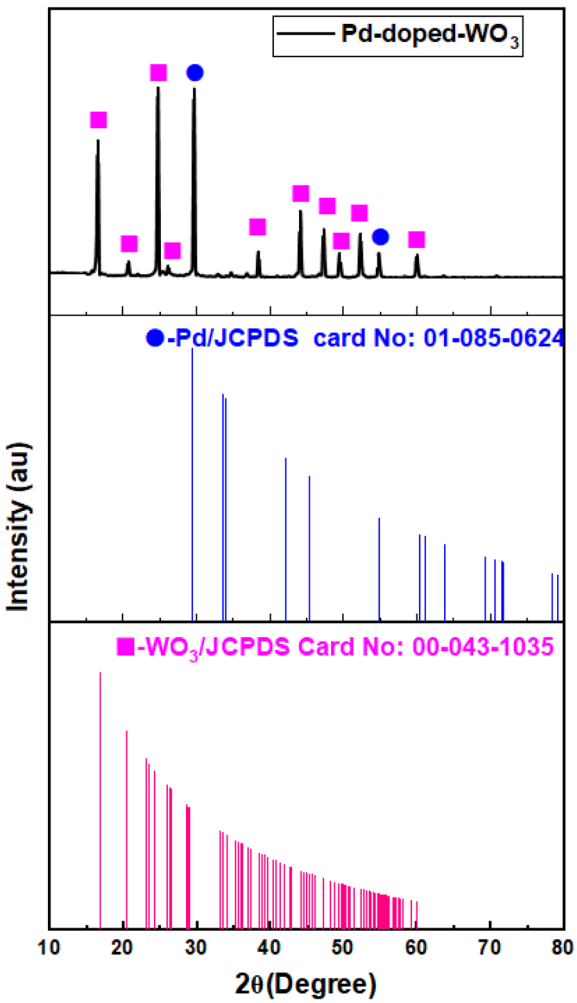

Fig. 2 XRD spectrum of Pd-doped-WO_3 nanocomposite synthesized using *Anisomeles indica* extract.

advantageous for catalytic applications due to enhanced surface properties and active site exposure.

This analysis confirms the formation of a Pd-doped-WO_3 structure with the distinct monoclinic crystalline features of WO_3 along with metallic Pd, validating the effectiveness of the green synthesis approach.

4.1.3 SEM. The SEM was employed to examine the morphology and surface arrangement of the nanoparticles. Fig. 3(a) shows that the synthesized Pd nanoparticles have a compact, granular structure with a relatively uniform particle distribution. This nanostructured morphology offers enhanced surface exposure and catalytic potential.

In Fig. 3(b), the Pd-doped WO_3 nanocomposite exhibits a distinctly different surface architecture, characterized by irregular, aggregated particles and a rougher texture. This indicates the successful incorporation of Pd into the WO_3 framework, resulting in a composite structure. The presence of Pd on the WO_3 surface increases the number of catalytically active sites and improves electron transfer, which can significantly enhance the catalytic activity. The increased surface area and heterogeneous morphology of the nanocomposite are beneficial for promoting efficient interactions with the reactants during the Petasis reaction.

4.1.4 EDX. EDX analysis provides elemental composition details of the synthesized Pd-doped-WO_3 nanocomposite (Fig. 4). The spectrum confirms the presence of palladium (Pd), tungsten (W), and oxygen (O) as the primary elements, validating the successful formation of the Pd-doped-WO_3 nanocomposite. The detection of signals for Pd and W confirms that palladium has been effectively loaded onto the WO_3 matrix. Additionally, the atomic percentage analysis reveals that oxygen is the major element (77.93%), followed by tungsten (20.77%) and palladium (2.29%), indicating a dominant WO_3 framework with a modest but significant incorporation of Pd. These elemental ratios or composition are consistent with the expected stoichiometry of the composite and support the uniform

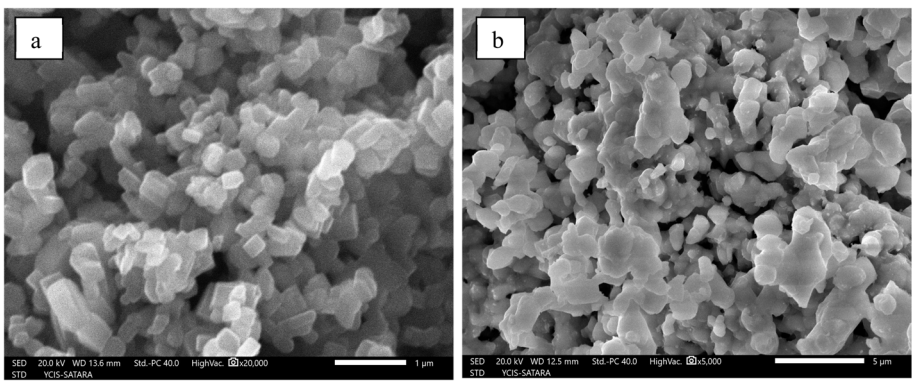

Fig. 3 (a) SEM image of synthesized Pd NPs, (b) Pd-doped-WO_3 nanocomposite.

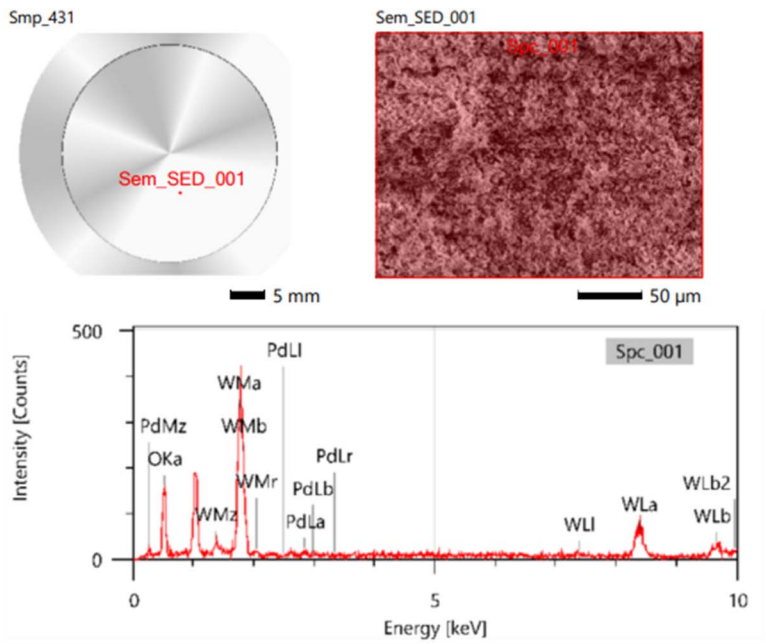

Signal SED
Landing Voltage 20.0 kV
WD 12.5 mm
Magnification x500
Vacuum Mode HighVacuum

Items	Value
measurement conditions	
Acceleration voltage	20.00 kV
Probe current	-
Magnification	x 500
Process time	T4
Measurement detector	First
Live time	30.00 seconds
Real time	31.08 seconds
Dead time	3.00 %
Count rate	585.00 CPS

Display name	Standard data	Quantification method	Result Type
Spc_001	Standardless	ZAF	Metal

Element	Line	Mass%	Atom%
O	K	23.96±0.81	77.93±2.64
Pd	L	4.65±0.43	2.29±0.21
W	M	71.39±1.87	20.77±0.53
Total		100.00	100.00
Spc_001			Fitting ratio 0.3572

Fig. 4 EDAX spectrum of Pd-doped-WO_3 nanocomposite.

distribution of Pd across the surface. Such a composition is crucial for catalytic applications, as the dispersion of Pd on the WO_3 surface can enhance the catalytic activity due to increased active sites and improved electron transfer. The presence of oxygen also suggests a stable oxide environment, beneficial for oxidation–reduction reactions.

Table S1 shows the various previously reported plant-mediated nanoparticles, while the present work demonstrates the synthesis of Pd-doped-WO_3 nanoparticles using *Anisomeles indica* leaf extract. Table 1 shows the previously used different catalysts for the synthesis of alkylaminophenols, from which we can conclude that the earlier palladium catalysts required more than 12 hours to yield the product. To overcome this limitation, we introduced a new catalytic system, Pd-doped-WO_3, in the presence of a hydrotrope, which uses less palladium (Scheme 1). To support this, we optimized the catalyst loading percentage in the Petasis reaction, as shown in Fig. S1. It was observed that a 3 mol% catalyst gives a greater yield with a minimum amount of palladium. To confirm whether the WO_3 affects the product yield or not, we carried out the reaction using only WO_3, which gave only a trace amount of product.

As presented in Table S2, we initially explored various solvent systems such as DCM, toluene, ethanol, and glycerol; however, none of them yielded satisfactory results. To attain improved outcomes while adhering to green chemistry principles, we introduced a hydrotropic system. Additionally, to evaluate the influence of the hydrotrope, the reaction was conducted both in its presence and absence. We observed better results in the presence of a hydrotrope at 60 °C. When the reaction was done using Pd-doped-WO_3 without a hydrotrope, the yield was lower than with a hydrotrope. So, the optimized condition was found to be Pd-doped-WO_3, hydrotrope, at 60 °C. Furthermore, to find out the optimum concentration of hydrotrope, we optimized different conditions and observed that 20% NaPTS gave a better yield (Fig. S2).

Table 2 shows the synthesis of various alkylaminophenol derivatives catalysed by Pd-doped WO_3 nanocomposite in a 20% aqueous hydrotropic medium. The catalyst gave good to excellent yields, going up to 98%. Salicylaldehydes having electron-withdrawing groups (like $-NO_2$ or $-Cl$) helped in faster iminium ion formation by increasing the electrophilicity of the aldehyde. On the other hand, boronic acids with electron-donating groups (like –OMe or $-CH_3$) gave higher yields. This is because EDG makes boronic acid more reactive and migrates faster to the iminium carbon, especially when palladium coordinates in between. So overall, Pd-doped WO_3, along with a hydrotropic medium, gave an efficient and mild method for making these alkylaminophenol molecules (Scheme 2).

4.2 Mechanism

In the proposed Petasis reaction mechanism (Scheme 3), the Pd-doped WO_3 nanocomposite acts as a dual-functional catalyst, where both the WO_3 surface and Pd centres actively participate in triggering organic conversion. The surface of WO_3, enriched with Lewis acidic sites,[37,38] coordinates with the carbonyl oxygen of substituted salicylaldehyde, thereby increasing the electrophilicity of the aldehyde carbon and facilitating a faster nucleophilic attack by the amine. This leads to the formation of a hemiaminal intermediate, which subsequently dehydrates into an iminium ion. Meanwhile, the *ortho*-hydroxyl group of salicylaldehyde interacts with the palladium sites on the catalyst surface, creating a bridge that brings the boronic acid into close proximity. This interaction aligns and activates the

Table 1 Comparison of previously reported catalysts for the Petasis reaction and screening of the prepared nanoparticles for the synthesis of alkylaminophenol derivatives

Entry	Catalyst	Conditions	Time	Yield %	References
1	$Pd(TFA)_2$ (5–10 mol%)	CH_3NO_2, 40 °C	64 h	45–99	29
2	Fe_3O_4@GO@AG@Cu^{II}	Solvent free, 120 °C	30 min	90	30
3	CuO NPs/RGO composite (10 wt%)	CH_2Cl_2, 70 °C, MW (400 W)	7 min	93	31
4	$CoFe_2O_4$ (15 mol%)	CH_3CN, 80 °C	2 h	90	32
5	Zn_2Ln_2 coordination clusters	DMF, RT	12–16 h	84–98	33
6	Nano Fe_3O_4 (2 mol%)	Dry dioxane, RT, 1–3 h	1–3 h	82–94	34
7	$H_2Ti_3O_7$ nanotubes (20 mg, TNT)	60°C	1 h	87–96	35
8	$Pd(TFA)_2$(10 mol%)	$MeNO_2$/DMSO 60 °C	12 h	53–81	36
9	**Pd-doped WO_3 NPs**	**Aq. NaPTS hydrotropic medium, 60 °C**	**1 h**	**98**	**Present work**

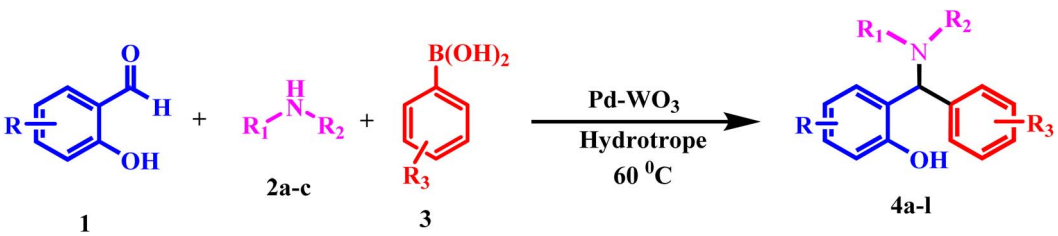

Scheme 1 Synthesis of alkylaminophenols.

Table 2 Synthesis of alkylaminophenol derivatives in 20% aqueous hydrotropic medium

Entry no.	Aldehyde	Amines	Boronic acid	Product	Yield	Time (hour)
1	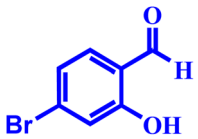	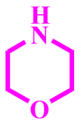	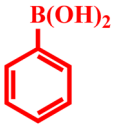	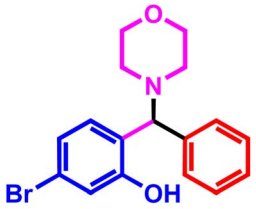 **4a**	98	1.03 h
2	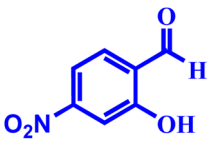	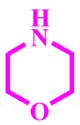	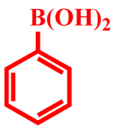	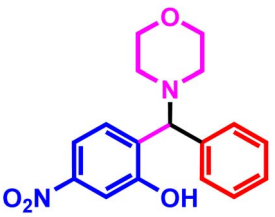 **4b**	98	1.00 h
3	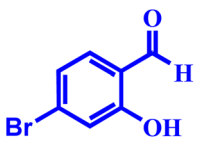	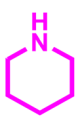	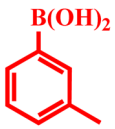	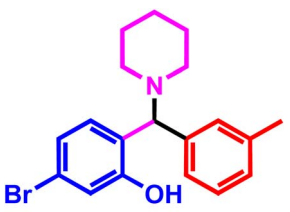 **4c**	97	1.05 h
4	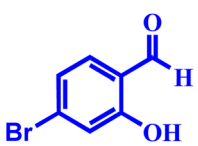	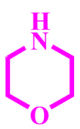	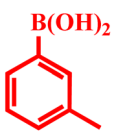	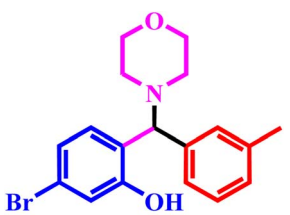 **4d**	98	1 h
5	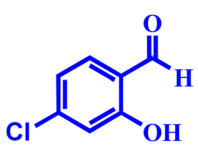	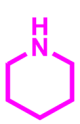	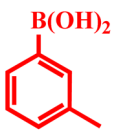	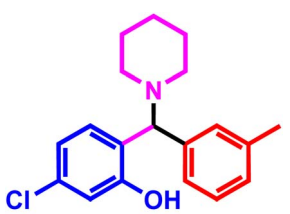 **4e**	97	1.05 h
6	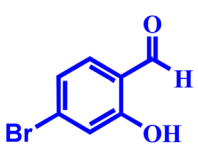	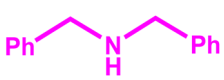	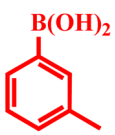	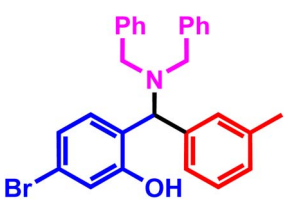 **4f**	96	1.08 h

Table 2 (*Contd.*)

Entry no.	Aldehyde	Amines	Boronic acid	Product	Yield	Time (hour)
7	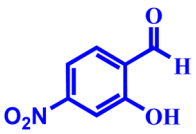		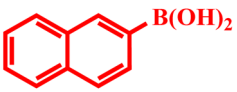	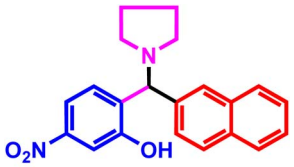 **4g**	97	1.08 h
8	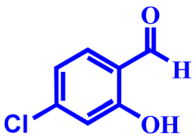		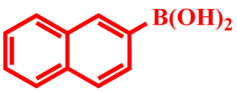	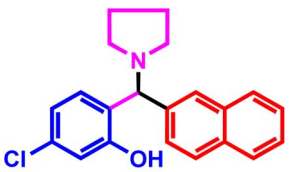 **4h**	96	1.10 h
9	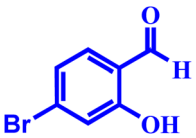		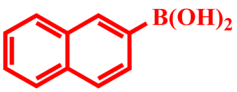	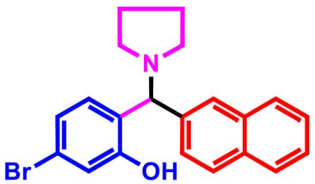 **4i**	97	1.10 h
10	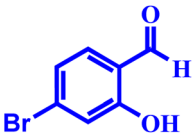	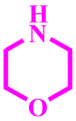	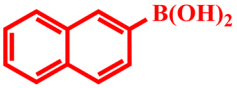	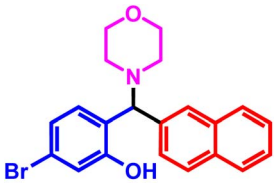 **4j**	96	1.10 h
11	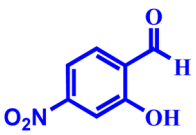	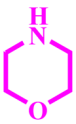		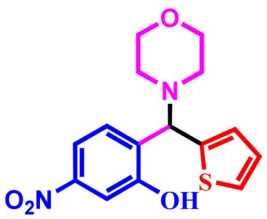 **4k**	97	1.08 h
12	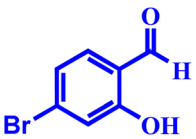	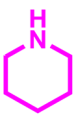	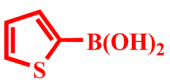	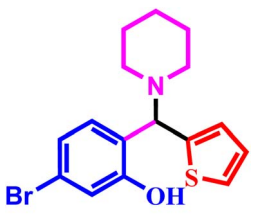 **4l**	96	1.08 h

Table 2 (*Contd.*)

Entry no.	Aldehyde	Amines	Boronic acid	Product	Yield	Time (hour)
13	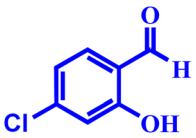	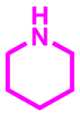		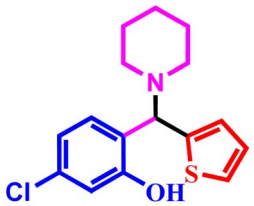 **4m**	96	1.10 h
14	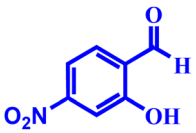	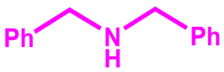	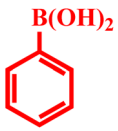	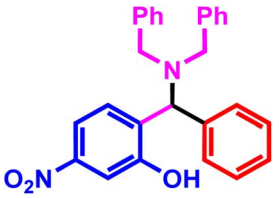 **4n**	98	1.00 h
15	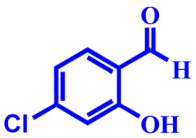	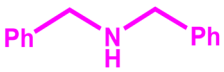	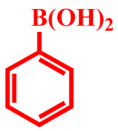	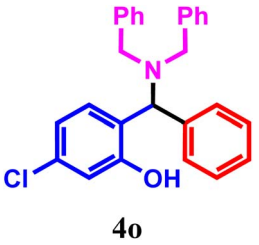 **4o**	97	1.03 h

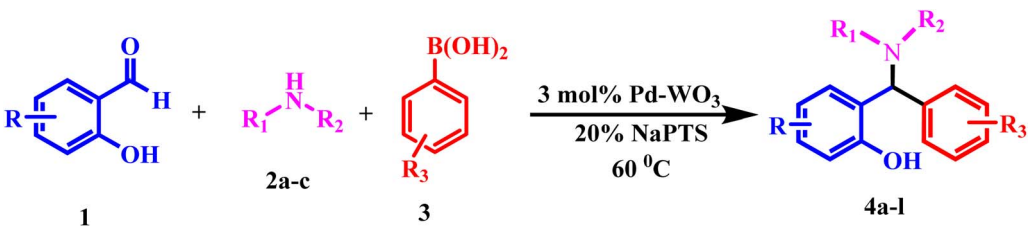

Scheme 2 Synthesis of alkylaminophenol derivatives in 20% aqueous hydrotropic medium.

boronic acid for efficient alkyl (or aryl) transfer to the electrophilic iminium ion carbon. The Pd nanoparticles dispersed on the WO_3 matrix thus provide active catalytic centres that mediate this transfer, while the WO_3 surface ensures continuous activation of the aldehyde. The synergistic interplay between WO_3 surface acidity and Pd-mediated bond formation accelerates C–C coupling and results in high catalytic efficiency under green hydrotropic conditions. Furthermore, SEM–EDX and XRD analyses confirmed the well-dispersed Pd nanoparticles on the WO_3 matrix, supporting the availability of active surface sites responsible for this enhanced catalytic performance.

4.3 Atom economy

The atom economy values presented in Table S3 highlight the efficiency of the Petasis reaction for the synthesis of alkylaminophenol derivatives (**4a–4o**) catalyzed by Pd-doped WO_3. The calculated atom economy values range from 83.27% to 88.43%, indicating that a substantial proportion of the reactant atoms are successfully incorporated into the final products, with minimal generation of by-products or waste.

Among the synthesized derivatives, compound **4f** exhibited the highest atom economy at 88.43%, suggesting highly efficient incorporation of all three reactants during the multicomponent coupling process. In contrast, compound **4m**

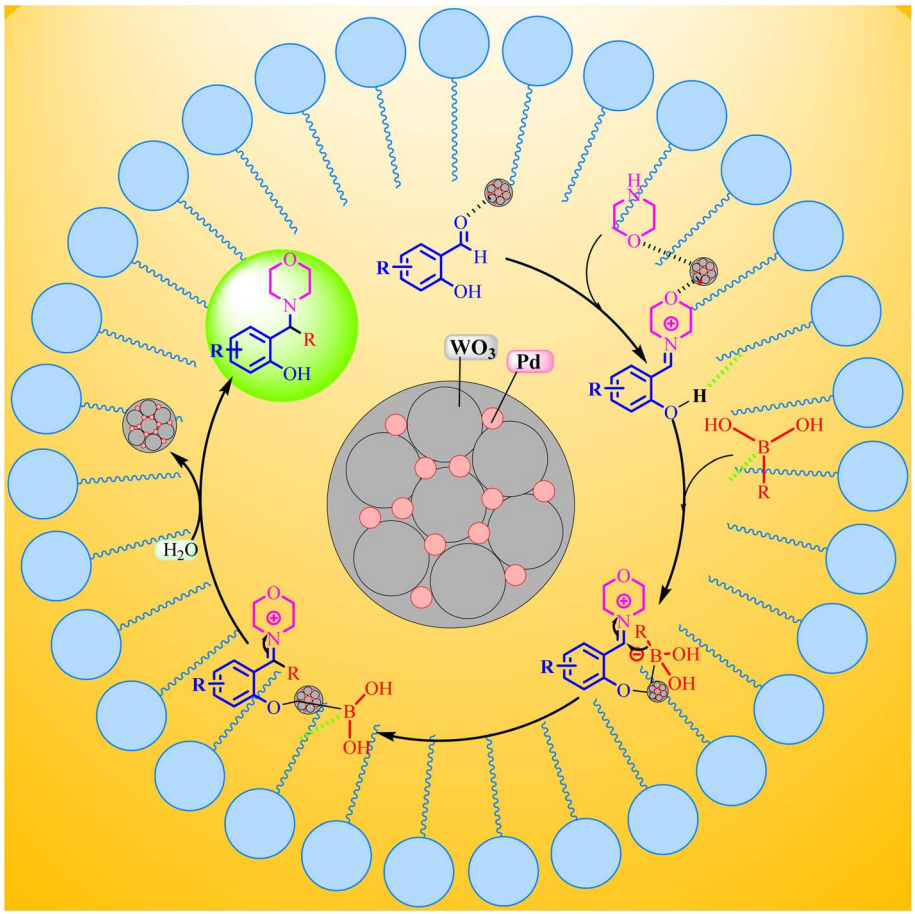

Scheme 3 Mechanism for the synthesis of alkylaminophenol derivatives.

showed the lowest atom economy at 83.27%, which could be attributed to the nature or bulkiness of specific substituents affecting the molecular mass balance or influencing minor side-product formation.

Overall, the consistently high atom economy values across the entire series reinforce the green and sustainable nature of this methodology. The use of a recyclable heterogeneous Pd–WO_3 nanocatalyst in an aqueous reaction medium further enhances the environmental compatibility of this synthetic route, aligning with the principles of atom-efficient and eco-friendly organic synthesis.

4.4 Turnover number and turnover frequency

The Pd-doped WO_3 nanocomposite catalyst demonstrated outstanding catalytic efficiency in the Petasis reaction, as evidenced by the turnover number (TON) and turnover frequency (TOF) values shown in Table S4. The TON values ranged from 13 190.4 to 13 465.2, reflecting the catalyst's ability to complete numerous catalytic cycles before deactivation. Similarly, the TOF values varied from 11 991.3 h^{-1} to 13 465.2 h^{-1}, indicating significant catalytic activity per unit time. Notably, products 4b,4d, 4n exhibited the highest TOF value (13 465.2 h^{-1}), suggesting that their electronic and steric characteristics, in conjunction with optimized reaction conditions, enhanced the turnover efficiency. Fig.S3 shows the consistent performance across various derivatives, further supporting the applicability of Pd-doped WO_3 as a robust and green nanocatalyst for efficient multicomponent reactions in environmentally friendly media.

4.5 Recyclability performance of Pd-doped-WO_3 and NaPTS

The recyclability performance of Pd-doped-WO_3 and the hydrotropic medium (NaPTS) was evaluated over five consecutive catalytic cycles, as illustrated in Fig. 5. Initially, both

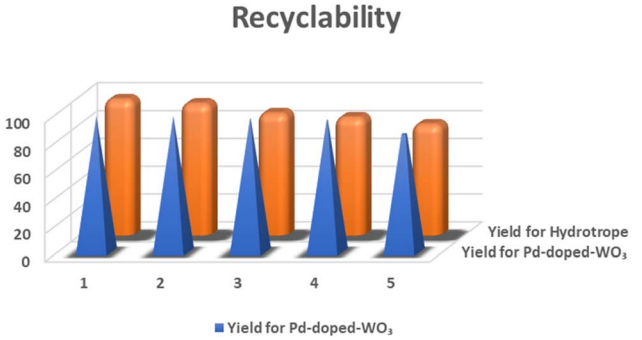

Fig. 5 Recyclability data showing yield (%) of Pd-doped-WO_3 and NaPTS over five consecutive cycles.

catalytic systems exhibited excellent yields of 98% in the first cycle, confirming their high activity. However, upon repeated use, a gradual decrease in yield was observed for both systems. Pd-doped-WO_3 showed slightly superior stability, maintaining 95% yield in the fourth run and 85% in the fifth, whereas the hydrotrope system showed a more significant decline, dropping to 85% and 80% in the fourth and fifth cycles, respectively. These results highlight the enhanced durability and recyclability of Pd-doped-WO_3 compared to the hydrotropic medium, demonstrating its potential as a robust heterogeneous catalyst for sustainable organic transformations.

4.6 Photocatalytic activity of Pd-doped-WO_3 NCs

In the present work, we have studied the photocatalytic performance of fungus-mediated Pd-doped-WO_3 NCs. Depending on the photocatalytic activity working principle, different NPs such as Fe, Ag, Au, Se, Cu, and ZnO are used for dye degradation. The MB degradation mechanism using the Pd-doped-WO_3 catalyst is explained below. In this degradation reaction mechanism, when a photon strikes the catalyst with energy comparable to the band gap of Pd-doped-WO_3, holes and electrons are created at the valence band and conduction band, respectively. The holes in the valence band form OH^- radicals, due to an oxidation reaction with H_2O molecules, while the electrons in the conduction band produce superoxide radicals O_2^-. Also, the dye's organic matter initiates a reaction with this OH^- radical that results in the formation of an intermediate product. This intermediate product then undergoes a reaction with a superoxide ion to generate peroxide or hydrogen peroxide, which results in the creation of water molecules.[39]

The photocatalytic reaction occurring at the valence band and conduction band of the Pd-doped-WO_3 nanocomposite can be explained as follows (eqn (3)–(9)):

$$PdWO_3 + h\nu \rightarrow PdWO_3(e^- + h^+) \quad (3)$$

$$h^+ + \text{dye} \rightarrow \text{product oxidation} \quad (4)$$

$$h^+ + H_2O \rightarrow OH^- + h^+ \quad (5)$$

$$OH^- + \text{dye} \rightarrow \text{degradation of product} \quad (6)$$

$$e^- + O_2 \rightarrow O_2^- \quad (7)$$

$$O_2^- + \text{dye} \rightarrow \text{degradation of product} \quad (8)$$

$$e^- + \text{dye} \rightarrow \text{reduction of product} \quad (9)$$

The photocatalytic potential of Pd-doped-WO_3 NCs for the remediation of MB dye was studied under sunlight irradiation.

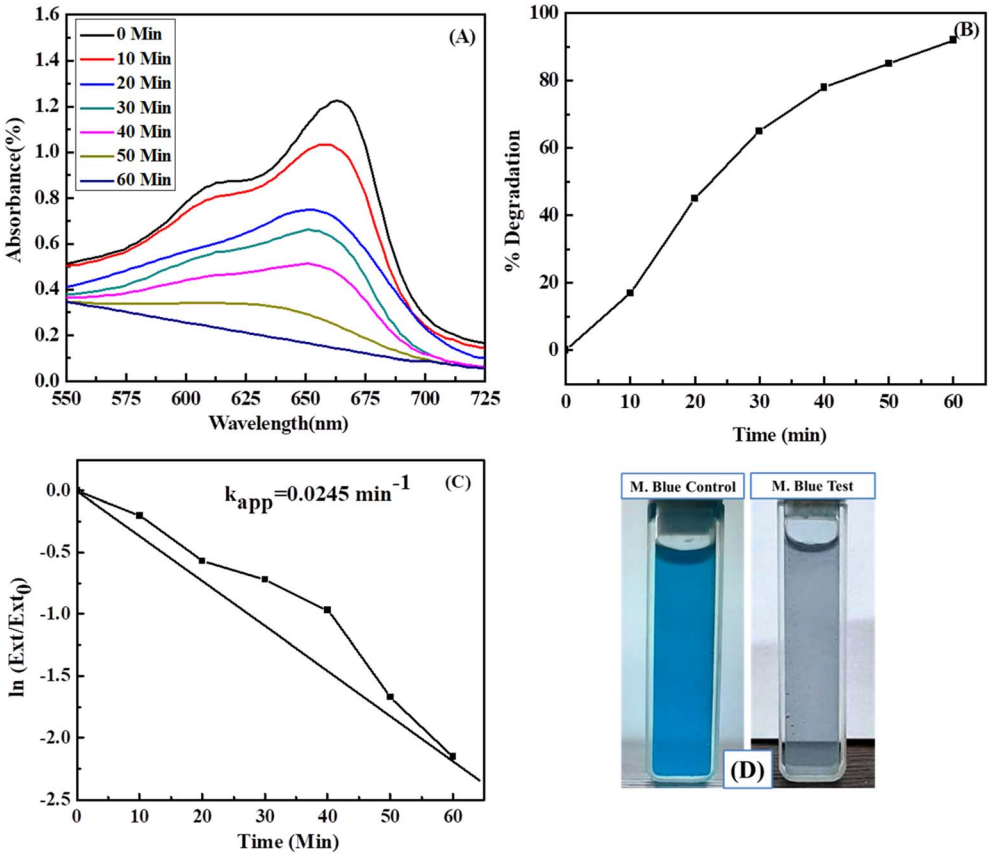

Fig. 6 (A) UV-visible absorption spectra of methylene blue dye using Pd-doped-WO_3 NCs at various time intervals. (B) Degradation % of methylene blue dye with time in the presence of Pd-doped-WO_3 material. (C) ln(C_t/C_0) *versus* degradation time plot for finding the reaction rate constant (k_{app}). (D) Show photographs of methylene blue before and after degradation.

It was monitored using UV-visible spectroscopy, shown in Fig. 6(A). The observed characteristic wavelength of the MB dye is 664 nm. An addition of Pd-doped-WO_3 NCs into the MB dye mixture results in gradual degradation of the dye and a colorless solution observed within a short interval (60 min). A progressive reduction in peak intensity maximum at 664 nm was detected, which reveals 90% degradation shown in Fig. 6(B). The Surface Plasmon Resonance (SPR) peak for Pd-doped-WO_3 NCs was not observed in the UV-visible spectrum during the catalytic study. From the plot of $\ln(C_t/C_0)$ *vs.* time, the rate constant (k_{app}) value was calculated, and it is found to be 0.0245 min^{-1} shown in Fig. 6(C). This indicates the reduction reaction follows pseudo-first-order kinetics and good linear correlation between $\ln(C_t/C_0)$ *vs.* time. Fig. 6(D) show photographs of before methylene blue dye remediation and after dye remediation.

4.7 Analysis of degraded products

4.7.1 TLC analysis. Fig. S4(a) depicts a one spot of MB that appears as a control and has a retardation factor (RF) value of 0.76. After complete decolonization, the degraded product develops as a single spot at a different location from the control, as shown in Fig. S4(b) with an RF value of 0.90. A co-sample is a mixture of pure dye and the degraded product, as shown in Fig. S4(c). Two spots appear at two distinct places that exactly match the locations of the pure and degraded samples. This confirms that methylene blue has been successfully degraded.

4.7.2 HPLC analysis. HPLC of MB (control) showed a sharp, intense peak of 3.798 min in Fig. S5(a), whereas the metabolites formed after 60 min degradation and decolorization showed five peaks at different retention times in Fig. S5(b). HPLC chromatogram of degraded metabolite showed significant peak variation in comparison to the standard dye, confirming photocatalytic remediation of methylene blue dye.

4.8 Biological evaluation

4.8.1 Antimicrobial activity. Table S5 presents a comparative analysis of the antimicrobial activities of various plant-mediated and conventionally synthesized Pd-based nanocomposites against different microbial strains. As observed, previously reported Pd–Mn_3O_4 and Pd–ZnO nanomaterials exhibited moderate inhibition zones ranging between 6–16 mm against both bacterial and fungal species. In contrast, the phyto-engineered Pd–WO_3 nanocomposite synthesized using *Anisomeles indica* leaf extract in the present study demonstrated markedly superior antibacterial performance, producing inhibition zones of 26 mm, 25 mm, 24 mm, and 22 mm against *Staphylococcus aureus*, *Bacillus cereus*, *Proteus vulgaris*, and *Salmonella typhimurium*, respectively. This significant enhancement in antibacterial efficiency can be attributed to the synergistic effect between Pd and WO_3, which facilitates enhanced reactive oxygen species (ROS) generation and disrupts microbial cell membranes more effectively. These results clearly indicate that the Pd–WO_3 nanocomposite developed in this work outperforms previously reported Pd-based nanomaterials, underscoring its potential as a promising antimicrobial agent.

The antimicrobial activity of green-synthesized Pd–WO_3 was checked along with blank distilled water as a negative control. The antimicrobial potential was studied using the agar well gel diffusion method against bacterial strains *S. aureus*, *B. cereus*, Gram-positive, *P. vulgaris*, and *S. typhimurium*, Gram-negative bacteria, using streptomycin as the standard antibiotic. These antibacterial studies revealed that Pd–WO_3 present in the well inhibits the growth of *S. aureus*, *B. cereus*, *P. vulgaris*, and *S. typhimurium*. The present study confirmed that the Pd-doped-WO_3 NPs have good antimicrobial activity compared to standard antibiotics, other nanomaterials and plant extracts against all tested pathogens. The above data represent the mean ± standard error of three replicates.[40–44]

The antibacterial performance of synthesized samples was evaluated against both Gram-positive and Gram-negative bacterial strains, including *Staphylococcus aureus* (NCIM-2654), *Bacillus cereus* (NCIM-2703), *Proteus vulgaris* (NCIM-2813), and *Salmonella typhimurium* (NCIM-2501). The results are presented as zones of inhibition (mm), reflecting the antimicrobial potency of each sample as shown in Table 3 and Fig. 7. Among the tested materials, the Pd-doped-WO_3 nanocomposite exhibited the highest antibacterial activity across all strains, showing inhibition zones ranging from 21.66 ± 0.57 mm to 25.66 ± 0.57 mm (Fig. S6). This superior performance is attributed to the synergistic effect between palladium and tungsten oxide, along with their enhanced surface reactivity and interaction with bacterial membranes. The plant extract

Table 3 Zone of inhibition of 1-WO_3 NPs, 2-Pd NPs, 3-plant extract, 4-Pd-doped-WO_3 NPs, and 5-antibiotic and C-control antimicrobial activity against human pathogens

	Antibacterial activity			
	Gram +ve		Gram −ve	
Entry	*Staphylococcus aureus* (NCIM-2654)	*Bacillus cerus* (NCIM – 2703)	*Proteus vulgaris* (NCIM – 2813)	*Salmonella typhimurium* (NCIM – 2501)
1-WO_3	13.66 ± 0.57	11.66 ± 0.57	11.66 ± 0.57	8.33 ± 0.57
2-Pd	15.66 ± 0.57	13.66 ± 0.57	12.33 ± 0.57	10.33 ± 0.57
3-Plant extract	15.33 ± 0.57	14.33 ± 0.57	12.33 ± 0.57	12.33 ± 0.57
4-Pd-doped-WO_3	25.66 ± 0.57	25.33 ± 0.57	23.66 ± 0.57	21.66 ± 0.57
5-Antibiotic	17.66 ± 0.57	17.66 ± 0.57	16.33 ± 0.57	17.66 ± 0.57

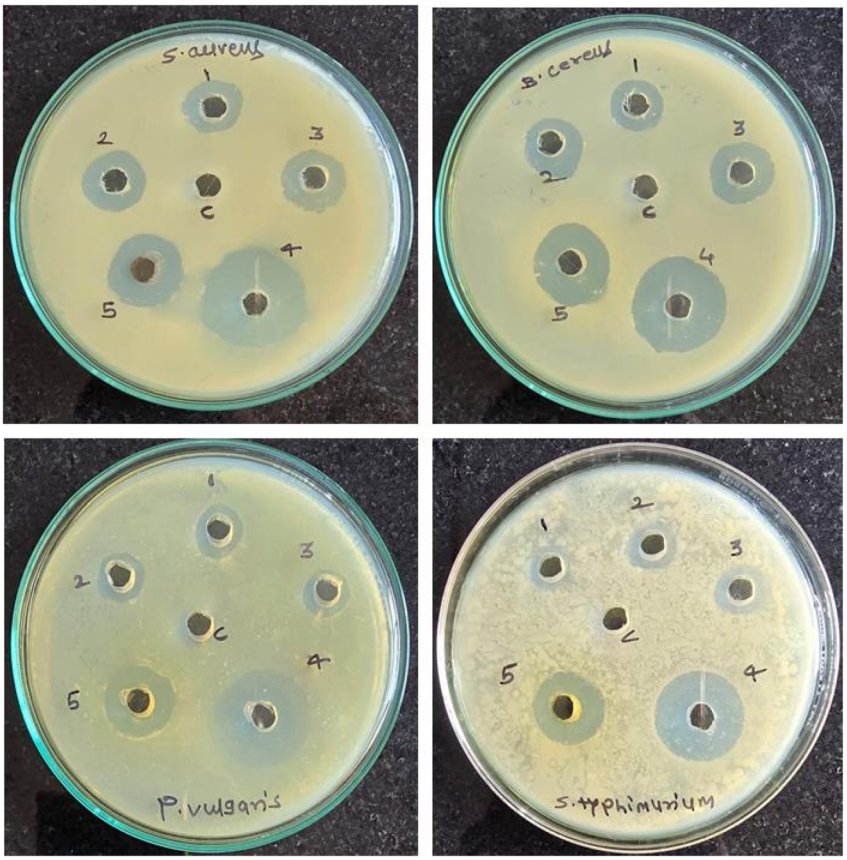

Fig. 7 Antimicrobial activity on the *Staphylococcus aureus* (NCIM-2654), *Bacillus cereus* (NCIM 2703), *Proteus vulgaris* (NCIM-2813), and *Salmonella typhimurium* (NCIM-2501) zone of inhibition for 1-WO_3 NPs, 2-Pd NPs, 3-plant extract, 4-Pd-doped-WO_3 NPs, and 5-antibiotic and C-control.

also showed moderate antimicrobial effects (12.33–15.33 mm), likely due to the presence of bioactive phytochemicals. Individually, WO_3 and Pd nanoparticles displayed relatively lower inhibition zones, indicating that their combination in a composite structure significantly enhances antibacterial properties. Interestingly, the Pd-doped-WO_3 nanocomposite outperformed the standard antibiotic control (which showed zones of 16.33–17.66 mm), suggesting its potential as a potent antimicrobial agent. These findings demonstrate that green-synthesized Pd-doped-WO_3 nanocomposites are not only effective catalysts but also promising candidates for antibacterial applications.

5 Conclusion

The present study demonstrates a green, sustainable, and efficient approach for synthesizing Pd-doped-WO_3 nanocomposites using *Anisomeles indica* leaf extract. The successful doping of palladium into the WO_3 matrix was confirmed through FTIR, SEM, EDX, and XRD analyses. The appearance of additional FTIR bands at 2932 and 1339 cm^{-1}, and XRD peaks at 2θ values of 29.380 and 55.020, further supported the incorporation of Pd into the WO_3 framework. The appearance of additional diffraction peaks aligning with the standard pattern of elemental palladium, particularly at 2θ values of 29.380 and 78.380, clearly confirms the successful incorporation of Pd into the composite, reinforcing the material's structural characterization. The synthesized nanocomposite exhibited excellent multifunctional performance, serving as an effective heterogeneous catalyst for the Petasis reaction under hydrotropic conditions, giving up to 98% yield, showing promising photocatalytic degradation of methylene blue dye (92.90%) within 60 minutes under sunlight, and demonstrating notable antibacterial activity against both Gram-positive and Gram-negative bacteria. The catalyst also showed high stability, low metal leaching, and reusability over multiple cycles without significant loss of activity. This work not only introduces a novel plant-mediated method for Pd-doped-WO_3 synthesis but also broadens its application scope across organic synthesis, environmental remediation, and biomedical fields, aligning with the principles of green chemistry.

Author contributions

Nilesh Pandit: methodology, conceptualization, investigation, formal analysis, writing – original draft, writing – review & editing. Avdhut Kadam: methodology, data curation, writing – review & editing. Avinash Survase: methodology, visualization, writing – original draft. Avdhut Patil: investigation, resources (plant collection). Prita Shara: investigation, software,

methodology. Sarika Patil: formal analysis, writing – review & editing. Santosh Kamble: resources, supervision, project administration, funding acquisition, writing – review & editing.

Conflicts of interest

There are no conflicts of interest to declare.

Data availability

All data supporting the findings of this study are included within the article and its supplementary information (SI). Additional raw data are available from the corresponding author upon reasonable request. Supplementary information is available. See DOI: **https://doi.org/10.1039/d5ra06905j**.

Acknowledgements

We sincerely appreciate the financial support provided by the Rayat Institute of Research and Development (RIRD) and Y.C.I.S. Satara (Autonomous). We also extend our gratitude to the Department of Science and Technology–Science and Engineering Research Board (DST-SERB) and the University Grants Commission (UGC) for their support of our major research projects.

References

1 J. Wang, B. Xu, S. Si, H. Li and G. Song, *Mol. Diversity*, 2014, **18**, 887–893.
2 S. R. Mane, S. K. Bais and S. R. Nigadi, *Energy*, 2023, 431–438.
3 N. T. Pandit, A. D. Kadam, S. S. Ghutukade, A. B. Ghode and S. B. Kamble, *J. Indian Chem. Soc.*, 2025, 101839.
4 N. T. Pandit and S. B. Kamble, *Top. Curr. Chem.*, 2025, **383**, 7.
5 S. Saeed, S. Munawar, S. Ahmad, A. Mansha, A. F. Zahoor, A. Irfan, A. Irfan, K. Kotwica-Mojzych, M. Soroka and M. Głowacka, *Molecules*, 2023, **28**, 8032.
6 C. Marques and P. Brandão, *Catalysts*, 2023, **13**, 1022.
7 G. Bosica and R. Abdilla, *Catalysts*, 2022, **12**, 725.
8 Y. K. Rao, S.-H. Fang, S.-C. Hsieh, T.-H. Yeh and Y.-M. Tzeng, *J. Ethnopharmacol.*, 2009, **121**, 292–296.
9 S. Ansari and M. P. Dobhal, *Pharmazie*, 1982, **37**, 453–454.
10 Y. K. Rao, S.-H. Fang, S.-C. Hsieh, T.-H. Yeh and Y.-M. Tzeng, *J. Ethnopharmacol.*, 2009, **121**, 292–296.
11 S. J. Sugitha, R. G. Latha, R. Venkatesan, A. A. Vetcher, N. Ali and S.-C. Kim, *Nanomaterials*, 2024, **14**, 1407.
12 M. Modak, S. Rane and S. Jagtap, *Bull. Mater. Sci.*, 2023, **46**, 28.
13 A. Fujishima, X. Zhang and D. A. Tryk, *Surf. Sci. Rep.*, 2008, **63**, 515–582.
14 H. Quan, Y. Gao and W. Wang, *Inorg. Chem. Front.*, 2020, **7**, 817–838.
15 L.-Y. Zhu, L.-X. Ou, L.-W. Mao, X.-Y. Wu, Y.-P. Liu and H.-L. Lu, *Nano-Micro Lett.*, 2023, **15**, 89.
16 S. Higashimoto, Y. Kurikawa, Y. Tanabe, T. Fukushima, A. Harada, M. Murata, Y. Sakata and H. Kobayashi, *Appl. Catal., B*, 2023, **325**, 122289.
17 Q. Xue, Y. Liu, Q. Zhou, M. Utsumi, Z. Zhang and N. Sugiura, *Chem. Eng. J.*, 2016, **283**, 614–621.
18 H. Lee, M. Kim, D. Sohn, S. Hun Kim, S.-G. Oh, S. Soon Im and I. Soo Kim, *RSC Adv.*, 2017, **7**, 6108–6113.
19 K. He, Z. Jin, X. Chu, W. Bi, W. Wang, C. Wang and S. Liu, *RSC Adv.*, 2019, **9**, 28439–28450.
20 Z. Han, J. Ren, J. Zhou, S. Zhang, Z. Zhang, L. Yang and C. Yin, *Int. J. Hydrogen Energy*, 2020, **45**, 7223–7233.
21 K. Sato, H. Yamashita and Y. Kojima, *Jpn. J. Appl. Phys.*, 2024, **63**, 04SP76.
22 B. Liu, D. Cai, Y. Liu, D. Wang, L. Wang, Y. Wang, H. Li, Q. Li and T. Wang, *Sens. Actuators, B*, 2014, **193**, 28–34.
23 R. P. Neethu and G. Madhu, *J. Mater. Sci.: Mater. Eng.*, 2025, **20**, 16.
24 M. Ranjbar, S. Fardindoost, S. M. Mahdavi, A. Iraji zad and N. G. Tahmasebi, *Sol. Energy Mater. Sol. Cells*, 2011, **95**, 2335–2340.
25 H. D. Shelke, A. R. Machale, A. A. Surwase, S. F. Shaikh, A. Rana and H. M. Pathan, *Coatings*, 2023, 522–533.
26 A. A. Survase and S. S. Kanase, *J. Mol. Struct.*, 2024, **1302**, 137421.
27 S. Iravani, *Green Chem.*, 2011, **13**, 2638–2650.
28 J. O. Tijani, O. Ugochukwu, L. A. Fadipe, M. T. Bankole, A. S. Abdulkareem and W. D. Roos, *Appl. Phys. A*, 2019, **125**, 162.
29 T. Beisel and G. Manolikakes, *Org. Lett.*, 2015, **17**, 3162–3165.
30 F. Rafiee and S. Hosseinvand, *Iran. J. Sci. Technol., Trans. A: Sci.*, 2021, **45**, 503–514.
31 A. Dandia, S. Bansal, R. Sharma, K. S. Rathore and V. Parewa, *RSC Adv.*, 2018, **8**, 30280–30288.
32 A. M. Kulkarni, K. S. Pandit, P. V. Chavan, U. V. Desai and P. P. Wadgaonkar, *RSC Adv.*, 2015, **5**, 70586–70594.
33 P. Kumar, K. Griffiths, S. Lymperopoulou and G. E. Kostakis, *RSC Adv.*, 2016, **6**, 79180–79184.
34 P. Chacko and K. Shivashankar, *J. Chem. Sci.*, 2018, **130**, 154.
35 B. R. Prasad Reddy, P. V. Govardhana Reddy, D. P. Kumar, B. N. Reddy and M. V. Shankar, *RSC Adv.*, 2016, **6**, 14682–14691.
36 A. M. Diehl and G. Manolikakes, *ChemCatChem*, 2020, **12**, 3463–3466.
37 H. Zhou, Z. Chen, F. Kong, Z. Dou, J. Hu and M. Wang, *Angew. Chem.*, 2025, e202516021.
38 S. Swain, N. Dey, S. Roy and B. M. Reddy, *Top. Catal.*, 2025, **68**, 2242–2254.
39 A. A. Survase, M. T. Mane, S. S. Kanase, P. R. Salunkhe, P. M. Gaikwad, V. S. Patil, A. D. Kadam, S. H. Sutar, P. S. Pawar and N. T. Pandit, *Interactions*, 2025, **246**, 70.
40 A. A. Survase and S. S. Kanase, *Ceram. Int.*, 2023, **49**, 14964–14980.
41 A. D. Kadam, A. C. Sapkal, A. A. Survase and S. B. Kamble, *ChemistrySelect*, 2024, e202400088.
42 H. D. Shelke, A. R. Machale, A. A. Surwase, S. F. Shaikh, A. u. H. S. Rana and H. M. Pathan, *Coatings*, 2023, **13**, 522.
43 A. A. Survase, M. T. Mane, S. S. Kanase, P. R. Salunkhe, P. M. Gaikwad, V. S. Patil, A. D. Kadam, S. H. Sutar, P. S. Pawar and N. T. Pandit, *Interactions*, 2025, **246**, 70.
44 S. S. Wagh, A. S. Chougale, A. A. Survase, R. S. Patil, N. Naik, M. Naushad and H. M. Pathan, *Sci. Rep.*, 2024, **14**, 14045.